

pubs.acs.org/JPCL Letter

Experimental Assessment of the Electronic and Geometrical Structure of a Near-Infrared Absorbing and Highly Fluorescent Microbial Rhodopsin

Matthias Broser,*,[∇] Tadeusz Andruniów,[∇] Anastasia Kraskov,[∇] Riccardo Palombo, Sagie Katz, Miroslav Kloz, Jakub Dostál, César Bernardo, John T. M. Kennis, Peter Hegemann, Massimo Olivucci,* and Peter Hildebrandt*



Cite This: J. Phys. Chem. Lett. 2023, 14, 9291–9295



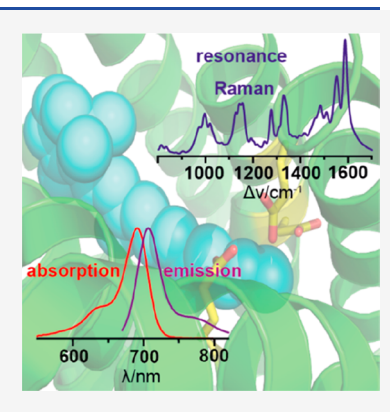
ACCESS

Metrics & More

Article Recommendations

Supporting Information

ABSTRACT: The recently discovered Neorhodopsin (NeoR) exhibits absorption and emission maxima in the near-infrared spectral region, which together with the high fluorescence quantum yield makes it an attractive retinal protein for optogenetic applications. The unique optical properties can be rationalized by a theoretical model that predicts a high charge transfer character in the electronic ground state (S_0) which is otherwise typical of the excited state S_1 in canonical retinal proteins. The present study sets out to assess the electronic structure of the NeoR chromophore by resonance Raman (RR) spectroscopy since frequencies and relative intensities of RR bands are controlled by the ground and excited state's properties. The RR spectra of NeoR differ dramatically from those of canonical rhodopsins but can be reliably reproduced by the calculations carried out within two different structural models. The remarkable agreement between the experimental and calculated spectra confirms the consistency and robustness of the theoretical approach.



n the past years, we have witnessed a renaissance of research lacksquare on microbial rhodopsin due to the discovery of new representatives from various species and prospective biomedical applications.^{1,2} In this context, the discovery of redlight-absorbing and highly fluorescent rhodopsins has raised widespread interest as "models" for engineering of more effective optogenetics tools. Moreover, on a fundamental level, such a discovery provides an opportunity to shed new light on how proteins control the properties of embedded chromophores. Despite their diverse functions, microbial rhodopsins share a similar structure and harbor a protonated retinal Schiff base (RSBH⁺) chromophore that is covalently bound to a cavity of the protein and absorbs light in the visible spectral range between 400 and 600 nm.³ The specific absorption maxima of the chromophore are determined by the interactions with the surrounding protein residues.^{4–8} Mainly carboxylates function as counterions and affect the energy levels of the delocalized RSBH⁺ π -electron system and may alter the low fluorescence quantum yield (FQY) between 10⁻⁵ and 10^{-3} , and the photoisomerization quantum yield of 0.2– 0.5 of microbial rhodopsins. 3,10-12

The canonical properties described above have been challenged by the discovery of neorhodopsin from *Rhizoclosmatium globosum* (NeoR), which features an unprecedented red-shifted absorption ($\lambda^a_{\rm exp} = 690$ nm), a dramatically increased FQY of 20%, ¹³ and a drastically reduced photoisomerization efficiency of $\sim 3 \times 10^{-4}$ (Figure S1). These

properties do not fit the explanatory models of canonical retinal proteins.

Recent hybrid quantum mechanics/molecular mechanics (QM/MM) studies have suggested that in NeoR, the electrostatic field of the protein induces substantial changes in both the RSBH+ ground (S0) and excited (S1) electronic states, 14 corresponding to a partial inversion of the covalent and charge-transfer character (cf. Supporting Information, Figure S3), which prevails in the S_0 and S_1 states of canonical rhodopsins, respectively. In canonical rhodopsins the S₀ electronic structure features a positive charge almost completely localized in the chromophore -C=N fragment while the S₁ electronic structure displays a positive charge delocalized along the chromophore backbone toward its β ionone ring. 15-17 Such an inversion in NeoR would explain the far-red-shifted spectrum, the FQY enhancement, and a reduced photoisomerization efficiency that yielded isomerization around the C7=C8 bond, ¹⁸ a process that can only occur as a marginal byproduct in canonical rhodopsins. However, these

Received: August 3, 2023 Accepted: September 28, 2023 Published: October 10, 2023





changes in the S_0 and S_1 electronic structures lack any experimental assessment.

The present study focuses on resonance Raman (RR) spectroscopy as the critical benchmark for characterizing the unusual NeoR electronic structure. RR spectroscopy is a powerful tool for investigating microbial rhodopsins and has been widely used to study the RSBH $^+$ structure and dynamics. The main observables of this technique are frequencies and intensities depending on the details of the S $_0$ and S $_1$ states. Thus, comparing the experimental RR with the spectra calculated within the framework of this theoretical approach provides an excellent test for its accuracy and consistency and may specifically verify or reject the postulated inversion in the electronic character of the S $_1$ and S $_0$ states.

The RR spectra of NeoR were measured at 80 K with 1064 nm excitation (Figure 1) to achieve sufficiently strong

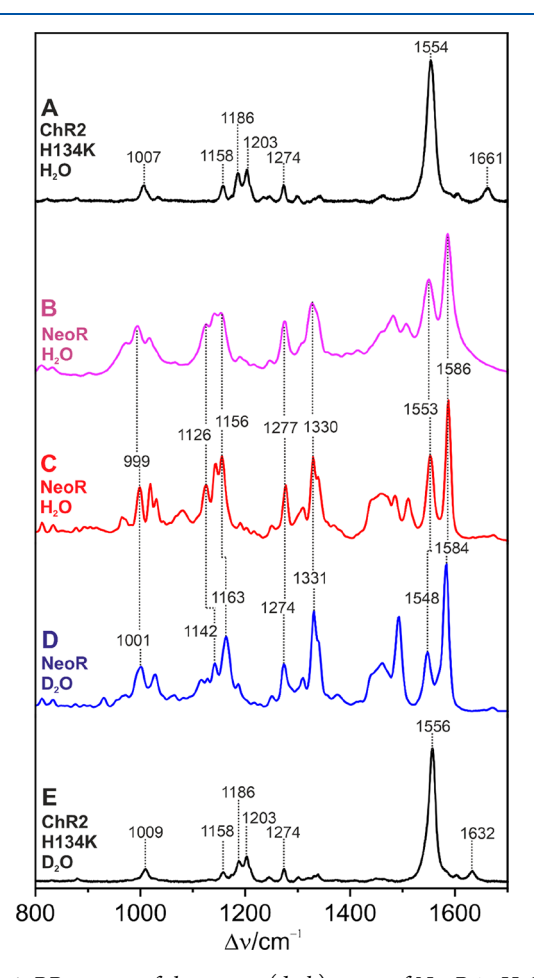


Figure 1. RR spectra of the parent (dark) states of NeoR in H_2O (C, red trace) and D_2O (D, blue trace) compared with those of canonical rhodopsin (ChR2-H134 K: A, E; black traces) from previous work. Trace B shows the stimulated Raman spectrum of NeoR measured with 800 nm excitation.

resonance enhancement, such that the spectra exclusively display the RR bands of RSBH⁺ without any interference from the protein. This is also illustrated by the agreement with the stimulated Raman spectrum, measured with a probe beam at 800 nm, 23 and thus even in closer resonance with the $S_0 \rightarrow S_1$ transition.

In comparison, Figure 1 also includes the RR spectrum of the all-trans isomer of dark-adapted channelrhodopsin-2

variant H134 K (ChR2-H134 K) measured under rigorous resonance conditions.²⁴ Most strikingly, the RR spectra of the two rhodopsins differ drastically. The RR spectrum of ChR2-H134 K, a type of canonical rhodopsin, is dominated by a single band at 1554 cm⁻¹. A small number of distinctly weaker bands between 1100 and 1300 cm⁻¹ accompanies it, and there are low-intensity bands at 1007 cm⁻¹, which is essentially invariant in all microbial rhodopsins and at 1661 cm⁻¹. In contrast, the RR spectrum of NeoR displays a complex band pattern between 900 and 1600 cm⁻¹ with a series of ~20 partially overlapping bands at strong and medium intensities. Also, the spectral changes upon H/D exchange at the Schiff base are strikingly different. While, for ChR2-H134 K, only very few bands are affected, with the furthest shift from 1661 to 1632 cm⁻¹ is observed for the C=N stretching of the protonated Schiff base. Significantly more spectral changes are noted in NeoR throughout the region from 900 to 1600 cm⁻¹ but no band attributable to the Schiff base (C15=N) stretching has been detected. In addition, all canonical rhodopsins studied so far obey a linear reciprocal relationship between the electronic absorption maximum and the frequency of the main band C=C stretching mode. 25,26 This relation holds for absorption wavelengths from the near-UV to the red and even for opsin-bound retinal analogues that absorb in the near-IR.7 Clearly, NeoR does not follow this relation.

We are primarily interested in the modes dominated by the C=C and C-C stretching coordinates of the polyene chain. Upon excitation in resonance with a strong electronic transition, the Franck-Condon mechanism (Albrecht's Aterm) holds, ^{19,27} and thus these modes should be associated with the highest RR intensities since the stretching coordinates are expected to display the highest excited-state displacement measurements Δd , i.e., the difference between the bond lengths in S₁ and S₀ ($\Delta d = d_{S0} - d_{S1}$). Hence, we consider Δd in more detail.

In canonical rhodopsins, the S_0 electronic structure of RSBH⁺ shows a covalent character and a positive charge residing in the Schiff base region. Such an electronic structure leads to the typical alternating double and single bond lengths of polyenes with negative and positive Δd for double and single bonds, respectively.²⁸ Therefore, the RR spectra show the highest intensity for the mode that involves the in-phase stretchings of essentially all C=C and C-C coordinates of the polyene chain (1554 cm⁻¹ in ChR2-H134 K).^{22,29} Additional modes involving C=C stretching coordinates are restricted to the region between 1500 and 1650 cm⁻¹, whereas modes with C-C but not C=C stretching character are clustered between 1100 and 1300 cm⁻¹.

The present calculations of the RR spectra rely on a QM/MM model (reported in ref 14, in the following referred to as MDR) built from a homology structure predicted by MODELLER³⁰ (see Section 1.3.2 in the Supporting Information), that has served as the basis for the computational modeling of NeoR in multiple studies. ^{13,14} The MDR model for NeoR reveals an unusual RSBH⁺ structure showing an alternating pattern of single and double bond lengths only in the region close to the β -ionone ring (i.e., C1=C6 to C9=C10). Instead, upon approaching the Schiff base terminus (C15=N), the length differences between single and double bonds decrease as the C12-C13 and C14-C15 bond lengths become shorter than those of the C13=C14 bond (Figure 2).

Concomitantly, in NeoR, the bond length alternation in the S_1 state is damped in the same direction from the β -ionone

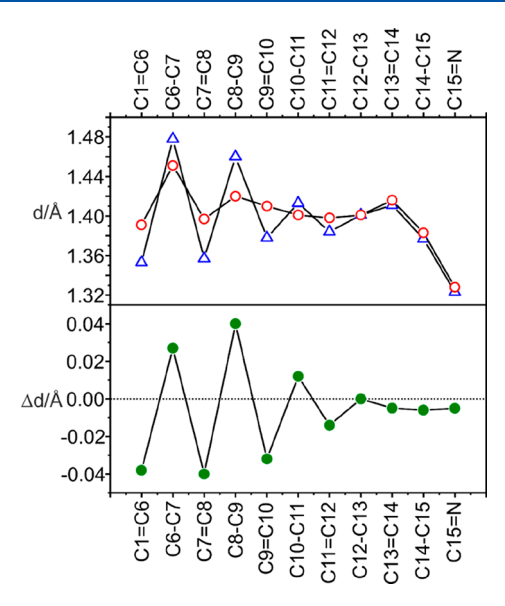


Figure 2. Top, calculated bond lengths of the polyene chain of the retinal chromophore of the MDR model. The open triangles and circles refer to the S_0 ground and S_1 excited states, respectively. Bottom, the bond length differences $\Delta d = d_{S0} - d_{S1}$ (green) representing the excited state displacements of the stretching coordinates. The red and blue colors refer to double and single bonds, respectively.

ring to the Schiff base, and thus Δd decreases and eventually approaches zero. Thus, the MDR model points to opsin electrostatics (i.e., residue charge distribution), creating a predominantly delocalized charge along the RSBH⁺ chain that can also be described in terms of a high percentage of charge transfer (CT) already in the S_0 state. Such a state refers to the typical S_1 charge distribution found in canonical rhodopsins where the positive charge, usually located on the chromophore -C=NH- moiety, is delocalized toward the β -ionone ring (see ref 16).

The unique electronic and structural properties of the S_0 and S_1 states of NeoR have distinct consequences for the RR spectra (Figure 3).

Both C=C and C-C stretchings contribute notably to a much greater number of normal modes in a large spectral region, from 1100 to 1650 cm⁻¹. Furthermore, the prominent RR bands are due to modes with significant contributions of two stretching coordinates on average. Among them is the C7=C8 stretching, which is involved in most of the modes with high RR intensity. Therefore, the intense band at 1586 cm⁻¹ observed in NeoR appears to be a consequence of the CT character of S₀ RSBH⁺. Notably, a mode with contributions of the C15=N stretching is calculated at 1646 cm⁻¹ (see Table S3) and thus at a frequency similar to that of canonical rhodopsins. However, consistent with the experimental observation, essentially no RR intensity is predicted for this mode, probably because the two main stretching coordinates involved (i.e., C15=N and C14-C15) have Δd values of nearly zero. In conclusion, the calculations reproduce the experimental RR spectra in both H₂O and D₂O solutions (Figure 3, Figure S7).

We carried out our calculations of NeoR using the previously reported MDR model, which was based on homology modeling (see Section 1.3.1 in the Supporting Information). To reduce any model-linked bias, we constructed a second QM/MM model (AP2) from a structure

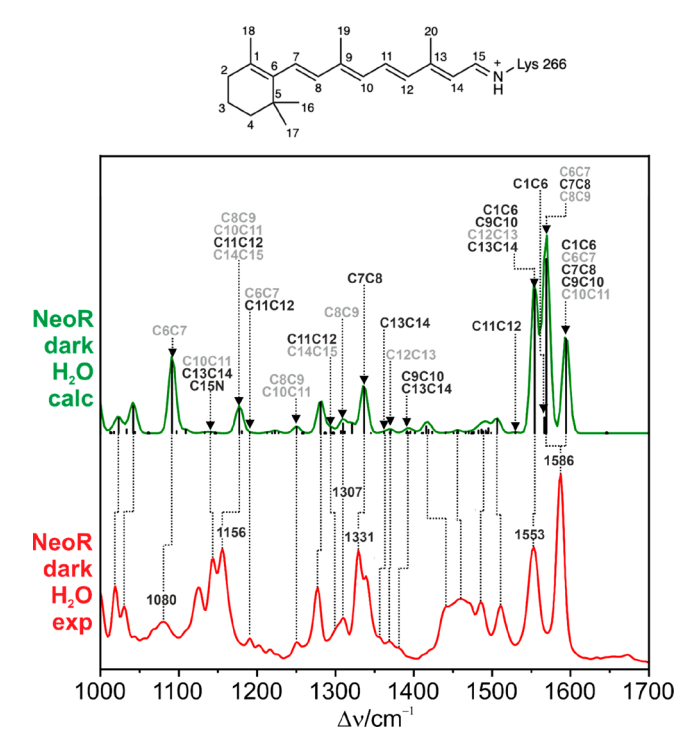


Figure 3. Calculated and experimental RR spectrum of NeoR in $\rm H_2O$. The calculated spectrum was generated by Gaussian band shapes of the vibrational transition derived from the QM partition of the MDR model (green trace). The spectrum also includes the line presentation of the vibrational transitions. Frequencies were scaled by a factor of 0.9. Modes with major C=C and C-C stretching characters (factoring to >50% of the contribution of a coordinate) are indicated by black and gray letters, respectively. The notation follows the numbering of the structural formula on top of the figure. Details of the calculated RSBH⁺ modes are listed in Table S3 (Supporting Information, Section 3.2).

predicted by AlphaFold2.31 The main differences between the two models refer to residues E141 and W234. In the MDR model, E141 is deprotonated (anionic), hydrogen bonded to W234, and points away from RSBH⁺. In the AP2 model, E141 is neutral and approaches closer to the RSBH⁺ (Figure 4; Figure S2). This different charge distribution leads to increased localization of the positive charge on the Schiff base unit in MDR concerning AP2, likely causing the slightly different bond length pattern in the Schiff base region (Figure 2, Figure S3; a comprehensive comparison of both models is given in the Supporting Information). The different bond length pattern specifically refers to the C14-C15 and C15=N bonds for which the MDR model yields $\Delta d \approx 0$ in contrast to the appreciable Δd value derived from the AP2 model (Figure S4). As a result, only the MDR model correctly predicts the lack of RR intensity for the Schiff base stretching mode at 1648 cm⁻¹ (vide supra). However, besides this mode, the AP2 model also provides a satisfactory simulation of the experimental RR spectra (Figures S8 and S9).

In both models, the S_1 potential energy surface (PES) mapping shows high energy barriers (E_{S1}^f) along both the canonical C13=C14 and C11=C12 photoisomerization paths (reported in Figure S6). This promptly explains the dramatic increase in FQY assigned to a hindered S_1 isomerization motion. A high E_{S1}^f also points to the opening of alternative C7=C8 and C9=C10 isomerization routes present in the MDR and AP2 models associated with the

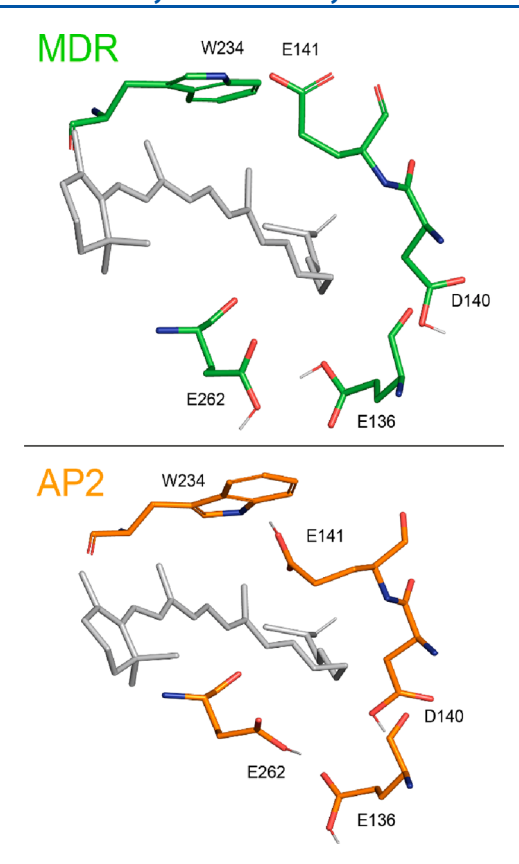


Figure 4. NeoR retinal binding cavities of the MDR and the AP2 model, with E136, D140, and E262 protonated in both models. In the MDR, deprotonated E141 forms a hydrogen bond with W234. This interaction is missing in AP2 with protonated (neutral) E141 (for more details, see Figure S2).

lowest barriers, even though they still amount to $\sim \! 15 \text{ kcal/mol}$ E^f_{S1} (Table S1). This prediction is in line with the photoisomerization from all-*trans* to 7-cis upon irradiation of NeoR with red light (Figure S10), whereas no isomerization around the C13=C14 double bond could be detected. 18

In conclusion, this study provides experimental support for the unusual RSBH⁺ electronic structure of NeoR predicted by two different QM/MM models. The fact that the models reproduce the observed RR spectrum implies that the chromophore S₀ and S₁ electronic structures are well described. Thus, unlike canonical microbial rhodopsins, RgNeoR (R. globosum) and probably all related NeoRs exhibit an S₀ state with strong CT character, limiting a clear bond length alternation pattern to the segment close to the β -ionone ring. Conversely, the same theoretical methodology allows to reproduce the experimental RR spectra and excited state properties of canonical rhodopsins with their "classical" charge distribution in the ground and excited states. 16,17 The charge distribution in NeoR significantly impacts the S₁ geometrical displacement, progression, and, ultimately, its reactivity. The present results provide strong support for the "chromophore charge delocalization and confinement" mechanism underlying the origin of the NeoR high energy barrier along the C13=C14 photoisomerization path and explaining the observed unprecedented FQY value of this microbial rhodopsin. 13,14

ASSOCIATED CONTENT

Solution Supporting Information

The Supporting Information is available free of charge at https://pubs.acs.org/doi/10.1021/acs.jpclett.3c02167.

Additional experimental and computational details, materials, and methods, including a comparison of the MDR and AP2 models referred to in the text (PDF) Transparent Peer Review report available (PDF)

AUTHOR INFORMATION

Corresponding Authors

Matthias Broser — Institut für Biologie, Experimentelle Biophysik, Humboldt-Universität zu Berlin, D-10115 Berlin, Germany; orcid.org/0000-0002-7133-4548; Email: matthias.broser@hu-berlin

Massimo Olivucci — Dipartimento di Biotecnologie, Universitâ di Siena, S3100 Siena, Italy; Department of Chemistry, Bowling Green State University, Bowling Green, Ohio 43403, United States; orcid.org/0000-0002-8247-209X; Email: molivuc@bgsu.edu

Peter Hildebrandt — Institut für Chemie, Technische Universität Berlin, D-10623 Berlin, Germany; orcid.org/0000-0003-1030-5900; Email: peter.hildebrandt@tuberlin.de

Authors

Tadeusz Andruniów — Department of Chemistry, Wrocław University of Science and Technology, 50-370 Wrocław, Poland; orcid.org/0000-0002-2215-5287

Anastasia Kraskov – Institut für Chemie, Technische Universität Berlin, D-10623 Berlin, Germany

Riccardo Palombo – Dipartimento di Biotecnologie, Università di Siena, 53100 Siena, Italy

Sagie Katz – Institut für Chemie, Technische Universität Berlin, D-10623 Berlin, Germany

Miroslav Kloz – ELI Beamlines Facility, The Extreme Light Infrastructure ERIC, 25241 Dolní Břežany, Czech Republic Jakub Dostál – ELI Beamlines Facility, The Extreme Light

Infrastructure ERIC, 25241 Dolní Břežany, Czech Republic César Bernardo – ELI Beamlines Facility, The Extreme Light Infrastructure ERIC, 25241 Dolní Břežany, Czech Republic

John T. M. Kennis — Department of Physics and Astronomy, Faculty of Science, Vrije Universiteit Amsterdam, 1081 HV Amsterdam, The Netherlands; orcid.org/0000-0002-3563-2353

Peter Hegemann — Institut für Biologie, Experimentelle Biophysik, Humboldt-Universität zu Berlin, D-10115 Berlin, Germany; orcid.org/0000-0003-3589-6452

Complete contact information is available at: https://pubs.acs.org/10.1021/acs.jpclett.3c02167

Author Contributions

 $^{
abla}(ext{M.B.}, ext{T.A.}, ext{ and A.K.})$ These authors contributed equally.

The authors declare no competing financial interest.

ACKNOWLEDGMENTS

We thank Melanie Meiworm and Christina Schnick for their excellent technical assistance. This work was supported by the German Research Foundation, DFG Grant No. 509731234 to M.B., CRC1078 "Protonation Dynamics in Protein Function", project number 221545957, subproject B06 to P.Hi., and the

DFG under Germany's Excellence Strategy—EXC 311 2008/1 (UniSysCat)—390540038 (Research Unit E to P.He. and P.Hi.). P. He. acknowledges support from the European Research Council (ERC, Grant No. 951644-SOL) and from the Hertie Foundation (Hertie Professorship). M.O. acknowledges support from NSF CSDM-A Grant No. 2102619 and European-Union, Next Generation EU, MIUR Italia Domani Progetto mRNA Spoke 6 del "National Center for Gene Therapy and Drugs based on RNA Technology"—CUP B63C22000610006. M.K. acknowledges support from the Czech Science Foundation (Project No. 21-09692M). M.B., J.T.M.K., and P. He. acknowledge beam time access at ELI, Extreme Light Infrastructure ERIC.

REFERENCES

- (1) Kandori, H. Retinal Proteins: Photochemistry and Optogenetics. *Bull. Chem. Soc. Ipn.* **2020**, 93, 76–85.
- (2) Govorunova, E. G.; Koppel, L. A. The Road to Optogenetics: Microbial Rhodopsins. *Biochemistry (Mosc)* **2016**, *81* (9), 928–940.
- (3) Ernst, O. P.; Lodowski, D. T.; Elstner, M.; Hegemann, P.; Brown, L. S.; Kandori, H. Microbial and Animal Rhodopsins: Structures, Functions, and Molecular Mechanisms. *Chem. Rev.* **2014**, *114* (1), 126–163.
- (4) Kochendoerfer, G. G.; Verdegem, P. J.; van der Hoef, I.; Lugtenburg, J.; Mathies, R. A. Retinal Analog Study of the Role of Steric Interactions in the Excited State Isomerization Dynamics of Rhodopsin. *Biochemistry* **1996**, *35* (50), 16230–16240.
- (5) Engqvist, M. K.; McIsaac, R. S.; Dollinger, P.; Flytzanis, N. C.; Abrams, M.; Schor, S.; Arnold, F. H. Directed Evolution of Gloeobacter Violaceus Rhodopsin Spectral Properties. *J. Mol. Biol.* **2015**, 427 (1), 205–220.
- (6) McIsaac, R. S.; Engqvist, M. K.; Wannier, T.; Rosenthal, A. Z.; Herwig, L.; Flytzanis, N. C.; Imasheva, E. S.; Lanyi, J. K.; Balashov, S. P.; Gradinaru, V.; et al. Directed Evolution of a Far-Red Fluorescent Rhodopsin. *Proc. Natl. Acad. Sci. U.S.A.* **2014**, *111* (36), 13034–13039
- (7) Hontani, Y.; Ganapathy, S.; Frehan, S.; Kloz, M.; de Grip, W. J.; Kennis, J. T. M. Strong Ph-Dependent near-Infrared Fluorescence in a Microbial Rhodopsin Reconstituted with a Red-Shifting Retinal Analogue. *J. Phys. Chem. Lett.* **2018**, *9* (22), 6469–6474.
- (8) Laricheva, E. N.; Gozem, S.; Rinaldi, S.; Melaccio, F.; Valentini, A.; Olivucci, M. Origin of Fluorescence in 11-Cis Locked Bovine Rhodopsin. *J. Chem. Theory Comput.* **2012**, *8* (8), 2559–2563.
- (9) Penzkofer, A.; Silapetere, A.; Hegemann, P. Absorption and Emission Spectroscopic Investigation of the Thermal Dynamics of the Archaerhodopsin 3 Based Fluorescent Voltage Sensor Quasarl. *Int. J. Mol. Sci.* **2019**, 20 (17), 4086.
- (10) van Stokkum, I. H. M.; Hontani, Y.; Vierock, J.; Krause, B. S.; Hegemann, P.; Kennis, J. T. M. Reaction Dynamics in the Chrimson Channelrhodopsin: Observation of Product-State Evolution and Slow Diffusive Protein Motions. *J. Phys. Chem. Lett.* **2023**, *14* (6), 1485–1493.
- (11) Hontani, Y.; Marazzi, M.; Stehfest, K.; Mathes, T.; van Stokkum, I. H. M.; Elstner, M.; Hegemann, P.; Kennis, J. T. M. Reaction Dynamics of the Chimeric Channelrhodopsin C1C2. *Sci. Rep.* **2017**, *7* (1), 7217.
- (12) Malakar, P.; Das, I.; Bhattacharya, S.; Harris, A.; Sheves, M.; Brown, L. S.; Ruhman, S. Bidirectional Photochemistry of Antarctic Microbial Rhodopsin: Emerging Trend of Ballistic Photoisomerization from the 13-Cis Resting State. *J. Phys. Chem. Lett.* **2022**, *13* (34), 8134–8140.
- (13) Broser, M.; Spreen, A.; Konold, P. E.; Peter, E.; Adam, S.; Borin, V.; Schapiro, I.; Seifert, R.; Kennis, J. T. M.; Bernal Sierra, Y. A.; et al. Neor, a near-Infrared Absorbing Rhodopsin. *Nat. Commun.* **2020**, *11* (1), 5682.
- (14) Palombo, R.; Barneschi, L.; Pedraza-González, L.; Padula, D.; Schapiro, I.; Olivucci, M. Retinal Chromophore Charge Delocaliza-

- tion and Confinement Explain the Extreme Photophysics of Neorhodopsin. *Nat. Commun.* **2022**, *13* (1), 6652.
- (15) Yang, X.; Manathunga, M.; Gozem, S.; Léonard, J.; Andruniów, T.; Olivucci, M. Quantum-Classical Simulations of Rhodopsin Reveal Excited-State Population Splitting and Its Effects on Quantum Efficiency. *Nat. Chem.* **2022**, *14* (4), 441–449.
- (16) Gozem, S.; Luk, H. L.; Schapiro, I.; Olivucci, M. Theory and Simulation of the Ultrafast Double-Bond Isomerization of Biological Chromophores. *Chem. Rev.* **2017**, *117* (22), 13502–13565.
- (17) Bonačić-Koutecký, V.; Schöffel, K.; Michl, J. Critically Heterosymmetric Biradicaloid Geometries of Protonated Schiff Bases. *Theor. Chim. Acta* 1987, 72 (5), 459–474.
- (18) Sugiura, M.; Ishikawa, K.; Katayama, K.; Sumii, Y.; Abe-Yoshizumi, R.; Tsunoda, S. P.; Furutani, Y.; Shibata, N.; Brown, L. S.; Kandori, H. Unusual Photoisomerization Pathway in a near-Infrared Light Absorbing Enzymerhodopsin. *J. Phys. Chem. Lett.* **2022**, *13* (40), 9539–9543.
- (19) Buhrke, D.; Hildebrandt, P. Probing Structure and Reaction Dynamics of Proteins Using Time-Resolved Resonance Raman Spectroscopy. *Chem. Rev.* **2020**, *120* (7), 3577–3630.
- (20) Althaus, T.; Eisfeld, W.; Lohrmann, R.; Stockburger, M. Application of Raman Spectroscopy to Retinal Proteins. *Isr. J. Chem.* **1995**, 35 (3–4), 227–251.
- (21) Smith, S. O.; Lugtenburg, J.; Mathies, R. A. Determination of Retinal Chromophore Structure in Bacteriorhodopsin with Resonance Raman Spectroscopy. *J. Membr. Biol.* **1985**, *85* (2), 95–109.
- (22) Smith, S. O.; Braiman, M. S.; Myers, A. B.; Pardoen, J. A.; Courtin, J. M. L.; Winkel, C.; Lugtenburg, J.; Mathies, R. A. Vibrational Analysis of the All-Trans-Retinal Chromophore in Light-Adapted Bacteriorhodopsin. *J. Am. Chem. Soc.* **1987**, *109* (10), 3108–3125.
- (23) Kloz, M.; Weißenborn, J.; Polívka, T.; Frank, H. A.; Kennis, J. T. M. Spectral Watermarking in Femtosecond Stimulated Raman Spectroscopy: Resolving the Nature of the Carotenoid S* State. *Phys. Chem. Chem. Phys.* **2016**, *18* (21), 14619–14628.
- (24) Bruun, S.; Stoeppler, D.; Keidel, A.; Kuhlmann, U.; Luck, M.; Diehl, A.; Geiger, M.-A.; Woodmansee, D.; Trauner, D.; Hegemann, P.; et al. Light-Dark Adaptation of Channelrhodopsin Involves Photoconversion between the All-Trans and 13-Cis Retinal Isomers. *Biochemistry* **2015**, *54* (35), 5389–5400.
- (25) Doukas, A. G.; Aton, B.; Callender, R. H.; Ebrey, T. G. Resonance Raman Studies of Bovine Metarhodopsin I and Metarhodopsin II. *Biochemistry* 1978, 17 (12), 2430–2435.
- (26) Kajimoto, K.; Kikukawa, T.; Nakashima, H.; Yamaryo, H.; Saito, Y.; Fujisawa, T.; Demura, M.; Unno, M. Transient Resonance Raman Spectroscopy of a Light-Driven Sodium-Ion-Pump Rhodopsin from Indibacter Alkaliphilus. *J. Phys. Chem. B* **2017**, *121* (17), 4431–4437.
- (27) Albrecht, A. C. On the Theory of Raman Intensities. *J. Chem. Phys.* **1961**, 34 (5), 1476–1484.
- (28) Gozem, S.; Johnson, P. J. M.; Halpin, A.; Luk, H. L.; Morizumi, T.; Prokhorenko, V. I.; Ernst, O. P.; Olivucci, M.; Miller, R. J. D. Excited-State Vibronic Dynamics of Bacteriorhodopsin from Two-Dimensional Electronic Photon Echo Spectroscopy and Multiconfigurational Quantum Chemistry. J. Phys. Chem. Lett. 2020, 11 (10), 3889–3896.
- (29) Babitzki, G.; Mathias, G.; Tavan, P. The Infrared Spectra of the Retinal Chromophore in Bacteriorhodopsin Calculated by a DFT/MM Approach. *J. Phys. Chem. B* **2009**, *113* (30), 10496–10508.
- (30) Sali, A.; Blundell, T. L. Comparative Protein Modelling by Satisfaction of Spatial Restraints. *J. Mol. Biol.* **1993**, 234 (3), 779–815.
- (31) Jumper, J.; Evans, R.; Pritzel, A.; Green, T.; Figurnov, M.; Ronneberger, O.; Tunyasuvunakool, K.; Bates, R.; Žídek, A.; Potapenko, A.; et al. Highly Accurate Protein Structure Prediction with Alphafold. *Nature* **2021**, *596* (7873), 583–589.